Inorganic Chemistry
Article

Inorg. Chem. **2011**, *50*, 1767–1774 **1767**
DOI: 10.1021/ic102230r

Syntheses, Structure, and Luminescent Properties of Novel Hydrated Rare Earth Borates $Ln_2B_6O_{10}(OH)_4{\bullet}H_2O$ (*Ln* = Pr, Nd, Sm, Eu, Gd, Dy, Ho, and Y)

Rihong Cong,[†] Tao Yang,[†] Zheming Wang,[†] Junliang Sun,[‡] Fuhui Liao,[†] Yingxia Wang,*[,†] and Jianhua Lin*[,†]

[†]*Beijing National Laboratory for Molecular Sciences, State Key Laboratory of Rare Earth Materials Chemistry and Applications, College of Chemistry and Molecular Engineering, Peking University, Beijing 100871, P. R. China., and* [‡]*Structural Chemistry and Berzelii Centre, EXSELENT on Porous Materials, Stockholm University, SE-106 91, Stockholm, Sweden*

Received November 7, 2010

$Ln_2B_6O_{10}(OH)_4{\bullet}H_2O$ (*Ln* = Pr, Nd, Sm−Gd, Dy, Ho, and Y), a new series of hydrated rare earth borates, have been synthesized under hydrothermal conditions. A single crystal of Nd analogue was used for the structure determination by X-ray diffraction. It crystallizes in the monoclinic space group *C*2/*c* with lattice constants *a* = 21.756(4), *b* = 4.3671(9), *c* = 12.192(2) Å, and β = 108.29(3)°. The other compounds are isostructural to $Nd_2B_6O_{10}(OH)_4{\bullet}H_2O$. The fundamental building block (FBB) of the polyborate anion in this structure is a three-membered ring $[B_3O_6(OH)_2]^{5-}$. The FBBs are connected by sharing oxygen atoms forming an infinite $[B_3O_5(OH)_2]^{3-}$ chain, and the chains are linked by hydrogen bonds, establishing a two-dimensional (2-D) $[B_6O_{10}(OH)_4{\bullet}H_2O]^{6-}$ layer. The 2-D borate layers are thus interconnected by Ln^{3+} ions to form the complex three-dimensional structure. $Ln_2B_6O_{10}(OH)_4{\bullet}H_2O$ dehydrates stepwise, giving rise to two new intermediate compounds $Ln_2B_6O_{10}(OH)_4$ and $Ln_2B_6O_{11}(OH)_2$. The investigation on the luminescent properties of $Gd_{2-2x}Eu_{2x}B_6O_{10}(OH)_4{\bullet}H_2O$ (x = 0.01−1.00) shows a high efficiency of Eu^{3+} f−f transitions and the existence of the energy transfer process from Gd^{3+} to Eu^{3+}. $Eu_2B_6O_{10}(OH)_4{\bullet}H_2O$ and its two dehydrated products, $Eu_2B_6O_{10}(OH)_4$ and $Eu_2B_6O_{11}(OH)_2$, present the strongest emission peak at 620 nm ($^5D_0 \rightarrow {}^7F_2$ transition), which may be potential red phosphors.

1. Introduction

Rare earth borates have long been the subject of interest as hosts of luminescent materials for their high transparency, good thermal stability, and high luminescent efficiency.[1−3] In the $Ln_2O_3-B_2O_3$ (*Ln* = rare earth) system, three kinds of rare earth borates, including oxyborate,[4] orthoborate,[5,6] and metaborate[7,8] were identified by conventional solid state reaction. The revival in the synthesis of new rare earth borates was involved with new techniques, including high-pressure/high-temperature technique,[9−22] hydrothermal process,[23−28] and boric acid flux method.[29,30] The employment of the high pressure leads to, on one hand, a number of new polymorphs, such as χ-$LnBO_3$ (*Ln* = Dy, Er),[9] ν-$DyBO_3$,[10] β-LnB_3O_6 (*Ln* = Nd, Sm, Gd, Tb−Lu),[11,12] γ-LnB_3O_6 (*Ln* = La−Nd),[13] and δ-LnB_3O_6 (*Ln* = La, Ce),[14,15] and on the other hand, various rare earth borates with new compositions, for instances, $Ln_4B_6O_{15}$ (*Ln* = Dy, Ho),[16,17] α-$Ln_2B_4O_9$ (*Ln* = Sm−Ho),[18,19] β-$Ln_2B_4O_9$ (*Ln* = Dy, Gd),[20,21] and $Ln_3B_5O_{12}$ (*Ln* = Er−Lu).[22] Besides, hydrothermal and boric acid flux

*To whom correspondence should be addressed: E-mail: jhlin@pku.edu.cn (J.L.) and wangyx@pku.edu.cn (Y.W.). Phone: (8610)62751715. Fax: (8610)62751708.

(1) Saubat, B.; Fouassier, C.; Hagenmuller, P.; Bourcet, J. C. *Mater. Res. Bull.* **1981**, *16*, 193–198.
(2) Machida, K.; Adachi, G.; Shiokawa, J. *J. Lumin.* **1979**, *21*, 101–110.
(3) Pei, Z. W.; Su, Q.; Zhang, J. Y. *J. Alloys Compd.* **1993**, *198*, 51–53.
(4) Levin, E. M.; Robbins, C. R.; Waring, J. L. *J. Am. Ceram. Soc.* **1961**, *44*, 87–91.
(5) Lin, J. H.; Su, M. Z.; Wurst, K.; Schweda, E. *J. Solid State Chem.* **1996**, *126*, 287–291.
(6) Lin, J. H.; Zhou, S.; Yang, L. Q.; Yao, G. Q.; Su, M. Z.; You, L. P. *J. Solid State Chem.* **1997**, *134*, 158–163.
(7) Ren, M.; Lin, J. H.; Dong, Y.; Yang, L. Q.; Su, M. Z.; You, L. P. *Chem. Mater.* **1999**, *11*, 1576–1580.
(8) Yang, Z.; Ren, M.; Lin, J. H.; Su, M. Z.; Tao, Y.; Wang, W. *Chem. J. Chin. Univ.- Chinese* **2000**, *21*, 1339–1343.
(9) Huppertz, H.; von der Eltz, B.; Hoffmann, R. D.; Piotrowski, H. *J. Solid State Chem.* **2002**, *166*, 203–212.
(10) Emme, H.; Huppertz, H. *Acta Cryst. C* **2004**, *60*, I117–I119.
(11) Emme, H.; Nikelski, T.; Schleid, T.; Pöttgen, R.; Möller, M. H.; Huppertz, H. *Z. Naturforsch.* **2004**, *59b*, 202–215.
(12) Emme, H.; Heymann, G.; Haberer, A.; Huppertz, H. *Z. Naturforsch.* **2007**, *62b*, 765–770.
(13) Emme, H.; Despotopoulou, C.; Huppertz, H. *Z. Anorg. Allg. Chem.* **2004**, *630*, 2450–2457.
(14) Heymann, G.; Soltner, T.; Huppertz, H. *Solid State Sci.* **2006**, *8*, 821–829.
(15) Haberer, A.; Heymann, G.; Huppertz, H. *Z. Naturforsch.* **2007**, *62b*, 759–764.
(16) Huppertz, H.; von der Eltz, B. *J. Am. Chem. Soc.* **2002**, *124*, 9376–9377.
(17) Huppertz, H. *Z. Naturfors. B* **2003**, *58*, 278–290.
(18) Emme, H.; Huppertz, H. *Chem.—Eur. J.* **2003**, *9*, 3623–3633.
(19) Emme, H.; Huppertz, H. *Acta Cryst. C* **2005**, *61*, I29–I31.

Published on Web 01/21/2011

methods are also effective ways for obtaining new hydrous borates.[23−30] For example, LiNd[BO_3(OH)],[23] *Ln*[B_4O_6-(OH)$_2$]Cl (*Ln* = Pr, Nd),[24] GdH[B_2O_5],[25] NaNd[B_6O_9(OH)$_4$],[26] $LaB_5O_8(OH)_2$,[27] and $LaB_5O_8(OH)_2$•1.5H_2O[28] were obtained in the $Ln_2O_3-B_2O_3-H_2O$ system under hydrothermal conditions; *Ln*[B_5O_8(OH)]NO_3•3H_2O (*Ln* = La, Ce), *Ln*[B_6O_9-(OH)$_3$] (*Ln* = Sm−Lu), *Ln*[B_8O_{11}(OH)$_5$] (*Ln* = La−Nd), and *Ln*[B_9O_{13}(OH)$_4$]•H_2O (*Ln* = Pr−Er) were realized by using boric acid as both reaction reagent and reaction medium in $Ln_2O_3-H_3BO_3$ system.[29,30] The calcinations of the hydrated polyborates at moderate temperatures can give rise to the new anhydrous rare earth pentaborates, such as α-*Ln*B_5O_9 (*Ln* = Pr−Eu) and β-*Ln*B_5O_9 (*Ln* = La, Ce).[29,30]

In this paper, we shall present the study on the $Ln_2O_3-H_3BO_3-H_2O$ system. A new series of rare earth hydrous borates $Ln_2B_6O_{10}(OH)_4$•H_2O (*Ln* = Pr, Nd, Sm, Eu, Gd, Dy, Ho, and Y) was realized by careful control of the synthesis conditions. These compounds dehydrate stepwise, producing $Ln_2B_6O_{10}(OH)_4$ after the loss of the crystalline water molecule and then $Ln_2B_6O_{11}(OH)_2$ by the removal of half hydroxyl groups. The investigation on the luminescent properties of $Gd_{2-2}LnEu_{2x}B_6O_{10}(OH)_4$•$H_2O$ (x = 0.01−1.00) indicates these compounds are potential red phosphors.

2. Experimental Section

2.1. Synthesis. The syntheses of $Ln_2B_6O_{10}(OH)_4$•H_2O were carried out in closed Teflon autoclaves. The starting materials, H_3BO_3 and Ln_2O_3, were of analytical grade and used as obtained from commercial sources without further purification. Typically, 2.5 mmol of Ln_2O_3 (or 0.8 mmol Pr_6O_{11}) and 75 mmol of H_3BO_3 were first mixed and put into a 25 mL autoclave, then 7.5 mL of deionized water was added. The autoclave was sealed and heated at 220 °C in an oven for 3 days. The products were washed with water (25 °C) until the excess boric acid was completely removed and then dried at 80 °C for further characterization. The reaction conditions are relatively flexible. For example, the water amount is from 5 to 10 mL, and the temperature can vary between 180 and 220 °C. For *Ln* = Pr and Sm−Gd, pure $Ln_2B_6O_{10}(OH)_4$•H_2O samples can be obtained in a yield of ∼90% based on *Ln*; however, when *Ln* = Y, Dy, and Ho, an unknown phase (about 5−30 wt %) appears as an impurity when the reaction temperature is higher than 240−260 °C (See the powder XRD pattern in Figure S1 of the Supporting Information). The compounds $Ln_2B_6O_{10}$-(OH)$_4$•H_2O showed different colors: dark brown for Pr, light purple for Nd, light yellow for Sm and Ho, light pink for Eu, and colorless for Gd, Dy, and Y.

Table 1. Crystallographic Data and Structure Refinement Parameters for $Nd_2B_6O_{10}(OH)_4$•H_2O

formula	$Nd_2B_6O_{10}(OH)_4$•H_2O
formula mass	599.38
crystal size (mm)	0.10 × 0.09 × 0.03
morphology, color	flat-sheet, light purple
temperature (K)	293
crystal system	Monoclinic
space group	*C*2/*c*
a (Å)	21.756(4)
b (Å)	4.3671(9)
c (Å)	12.192(2)
β (deg)	108.29(3)
V (Å^3)	1099.9(4)
Z	4
ρ_{calcd}(g/cm^3)	3.62
λ (Å)	0.71073
μ (Mo K$_\alpha$) (mm^{-1})	9.431
θ range (deg)	3.45−27.50
number of reflections measured	7840
number of independent reflections	1267
number of observed reflections	1004
number of refined parameters	109
structure determination	Direct method
structure refinement	Shelx97
R_{int}	0.0692
final *R* indices [I > 2σ(I)]	R_1 = 0.0271 wR_2 = 0.0554
R indices (all data)	R_1 = 0.0380 wR_2 = 0.0569
GOF	1.000

In order to obtain appropriate single crystals for the structure determination, a smaller amount of starting materials, 0.5 mmol of Nd_2O_3, 7.5 mmol of H_3BO_3 (Nd/B = 1/15), and 2 mL of H_2O, were applied, and the reaction was performed under 240 °C for 3 days. The single crystals were present as flat sheets, and they were separated and kept in ethanol before data collection.

2.2. Structure Determination. A single crystal of $Nd_2B_6O_{10}$-(OH)$_4$•H_2O in the size of 0.10 mm × 0.09 mm × 0.03 mm was used for single-crystal X-ray diffraction data collection on a NONIUS Kappa-CCD using graphite-monochromated Mo Kα radiation (λ = 0.71073 Å) at 293 K. A total of 7840 reflections were collected in the region of 6.90° ≤ 2θ ≤ 55.00°, with −27 ≤ *h* ≤ 28, −5 ≤ *k* ≤ 5, −15 ≤ *l* ≤ 15, of which 1267 were independent and 1005 were observed ($I > 2\sigma$). Empirical absorption correction was applied.[31] The crystal structure was solved by direct method (SHELXS-97) and refined by full-matrix least-squares refinement.[32] All the Nd, B, and O atoms were refined anisotropically. The hydrogen atoms were added in riding model and refined isotropically. Detailed crystallographic information is listed in Table 1. The atomic coordinates, selected bond lengths, and angles are listed in Tables 2 and 3, respectively. CIF file and details of the structure are provided in the Supporting Information.

2.3. Characterization. Powder X-ray diffraction data for the refinements of cell parameters of the compounds $Ln_2B_6O_{10}$-(OH)$_4$•H_2O (*Ln* = Pr, Sm−Gd, Dy, Ho, and Y) and structure analysis of compounds $Sm_2B_6O_{10}(OH)_4$ and $Sm_2B_6O_{11}(OH)_2$, were collected at room temperature on Bruker Advance 8 diffractometer in a Debye−Scherrer geometry, using a curved germanium primary monochromated Cu Kα1 radiation (λ = 1.54059 Å, 40 kV and 40 mA). The collection conditions for the former are 2θ range of 7−80°, in step of 0.0197° with the remaining time 10 s/step, and for the latter are 2θ range of 7−120°, in step of 0.0197° with the remaining time 40 s/step. Powder X-ray diffraction data of the samples after the treatments at different

(20) Huppertz, H.; Altmannshofer, S.; Heymann, G. *J. Solid State Chem.* **2003**, *170*, 320–329.
(21) Emme, H.; Huppertz, H. *Acta Cryst. C* **2005**, *61*, I23–I24.
(22) Emme, H.; Valldor, M.; Pöttgen, R.; Huppertz, H. *Chem. Mater.* **2005**, *17*, 2707–2715.
(23) Abdyllayev, G. K.; Dzhafarov, G. G.; Mamedov, K. S. *Kristallografiya* **1984**, *29*, 1084–1088.
(24) Belokoneva, E. L.; Stefanovich, S. Y.; Dimitrova, O. V.; Ivanova, A. G. *Russ. J. Inorg. Chem.* **2002**, *47*, 317–323.
(25) Ivanova, A. G.; Belokoneva, E. L.; Dimitrova, O. V. *Russ. J. Inorg. Chem.* **2004**, *49*, 816–822.
(26) Belokoneva, E. L.; Ivanova, A. G.; Dimitrova, O. V. *Russ. J. Inorg. Chem.* **2006**, *51*, 869–877.
(27) Ivanova, A. G.; Belokoneva, E. L.; Dimitrova, O. V.; Mochenova, N. N. *Russ. J. Inorg. Chem.* **2006**, *51*, 584–588.
(28) Ivanova, A. G.; Belokoneva, E. L.; Dimitrova, O. V.; Mochenova, N. N. *Russ. J. Inorg. Chem.* **2006**, *51*, 862–868.
(29) Li, L. Y.; Lu, P. C.; Wang, Y. Y.; Jin, X. L.; Li, G. B.; Wang, Y. X.; You, L. P.; Lin, J. H. *Chem. Mater.* **2002**, *14*, 4963–4968.
(30) Li, L. Y.; Jin, X. L.; Li, G. B.; Wang, Y. X.; Liao, F. H.; Yao, G. Q.; Lin, J. H. *Chem. Mater.* **2003**, *15*, 2253–2260.
(31) Blessing, R. H. *Acta Cryst. A* **1995**, *51*, 33–38.
(32) Sheldrick, G. M. *SHELXS 97, Program for the Solution of Crystal Structures, and SHELXL 97, Program for the Refinement of Crystal Structures*; University of Göttingen: Göttingen, Germany, 1997.

Table 2. Atomic Coordinates and Isotropic Thermal Parameters of $Nd_2B_6O_{10}(OH)_4•H_2O$

atom	site	*x*	*y*	*z*	Ueq (Å^2)
Nd	8*f*	0.20252(1)	0.05199(7)	0.83259(2)	0.0129(1)
O1	8*f*	0.0821(2)	0.4634(8)	0.0016(3)	0.0175(8)
O2	8*f*	0.2419(2)	0.0652(8)	0.6641(3)	0.0135(7)
O3	8*f*	0.1591(2)	0.8376(9)	0.9744(3)	0.0151(8)
O4	8*f*	0.1239(2)	0.4441(8)	0.8392(3)	0.0151(8)
H1	8*f*	0.0852	0.4036	0.8124	0.023
O5	8*f*	0.1318(2)	0.9327(8)	0.6361(3)	0.0140(8)
O6	8*f*	0.0248(2)	0.2117(9)	0.1128(3)	0.0245(9)
H2	8*f*	0.9953	0.3138	0.0702	0.037
O7	8*f*	0.3055(2)	0.1685(8)	0.9691(3)	0.0129(7)
O8	4*e*	0	0.226(1)	0.75	0.023(1)
H3	8*f*	0.006(3)	0.08(1)	0.701(5)	0.04(2)
B1	8*f*	0.0797(3)	0.250(1)	0.0815(5)	0.016(1)
B2	8*f*	0.3176(3)	0.469(1)	0.9236(5)	0.011(1)
B3	8*f*	0.1395(3)	0.521(1)	0.9633(5)	0.013(1)

Table 3. Selected Bond Lengths and Angles for $Nd_2B_6O_{10}(OH)_4•H_2O$

atom−atom	bond lengths (Å)	atom−atom−atom	bond angles (deg)
Nd−O7	2.389(3)	O1−B1−O6	121.1(5)
Nd−O3	2.404(3)	O1−B1−O5	122.1(5)
Nd−O4	2.440(4)	O5−B1−O6	116.8(5)
Nd−O2	2.439(4)		
Nd−O2	2.463(4)	O3−B2−O2	116.6(4)
Nd−O5	2.463(3)	O3−B2−O7	104.4(4)
Nd−O2	2.541(4)	O2−B2−O7	108.0(4)
Nd−O7	2.762(3)	O3−B2−O5	111.3(4)
		O2−B2−O5	106.9(4)
B1−O1	1.360(7)	O7−B2−O5	109.4(4)
B1−O5	1.377(7)		
B1−O6	1.373(7)	O3−B3−O7	108.7(4)
		O3−B3−O4	106.2(4)
B2−O2	1.459(7)	O7−B3−O4	109.1(4)
B2−O3	1.457(7)	O3−B3−O1	112.8(4)
B2−O5	1.505(7)	O7−B3−O1	110.2(4)
B2−O7	1.480(7)	O4−B3−O1	109.7(4)
B3−O1	1.485(7)		
B3−O3	1.441(7)		
B3−O4	1.482(6)		
B3−O7	1.476(7)		

temperatures were collected on a Rigaku D/Max-2000 diffractometer using a rotating anode (Cu Kα, 40 kV and 100 mA), a graphite monochromator, and a scintillation detector.

The chemical analysis of $Nd_2B_6O_{10}(OH)_4•H_2O$ was conducted by the inductively coupled plasma method on a PROFILE SPEC atomic emission spectrometer, and the analysis result is Nd:B ≈ 1:3.05. Combined thermogravimetric analysis (TG) and mass spectra (MS) analysis of $Ln_2B_6O_{10}(OH)_4•H_2O$ were performed on a NETZSCH STA449C instrument at a heating rate of 10 °C/min from room temperature to 800 °C under Ar flow. FT-IR spectroscopies were measured on a NICOLET iN10 MX spectrum instrument. Luminescent spectra were measured on a HITACHI F4500 fluorescence spectrophotometer.

3. Results and Discussions

3.1. Synthesis of $Ln_2B_6O_{10}(OH)_4•H_2O$. The addition of an appropriate amount of water, 5−10 mL, is essential for the formation of the expected compounds; otherwise, other phases may emerge. For instance, the reaction of the mixture of Ln_2O_3 (2.5 mmol) and H_3BO_3 with *Ln*/B = 1/15 without additional water at about 220 °C led to a mixture of two known compounds $Ln[B_9O_{13}(OH)_4]•H_2O$ (*Ln* = Pr, Nd) and $Ln[B_6O_9(OH)_3]$ (*Ln* = Sm−Ho, Y);[29,30] when less than 5 mL water was added, the title compounds $Ln_2B_6O_{10}(OH)_4•H_2O$ were formed with $Ln[B_9O_{13}(OH)_4]•H_2O$ (*Ln* = Pr, Nd) or $Ln[B_6O_9(OH)_3]$ (*Ln* = Sm−Ho, Y) as admixture. If the added water amount is more than 10 mL, $LnBO_3$ or rare-earth hydroxides were obtained.

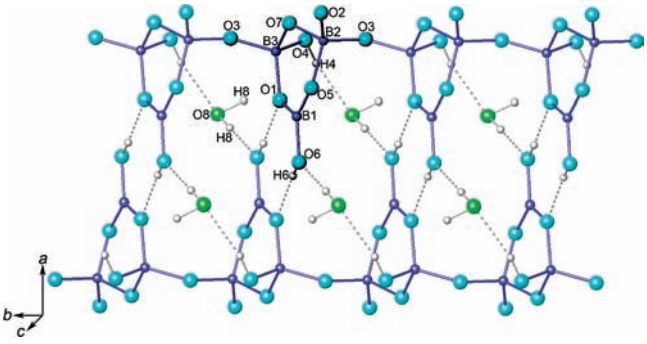

Figure 1. Borate chains and their connection by hydrogen bonds in $Nd_2B_6O_{10}(OH)_4•H_2O$. (The three-membered ring FBB $[B_3O_6(OH)_2]^{5-}$ is highlighted.)

3.2. Description of Crystal Structure. There are 12 crystallographically independent non-hydrogen atoms, including 1 Nd, 3 B, and 8 O. O8 is located in 2-fold axis (4*e* site), and others are all located in general positions. If only non-hydrogen atoms are considered, the chemical formula of the structure is $[Nd_2B_6O_{15}]^{6-}$. Apparently, six hydrogen atoms are needed to compensate the negative charges; therefore, hydrogen atoms were attached to O4, O6, and O8 during the refinement of single-crystal X-ray diffraction data. The bond valence sum (BVS) calculations also confirm the location of the hydrogen atoms: O4 and O6 have obvious low BVS values, (1.16 and 0.99, respectively), which are protonated by H1 and H2, respectively; O8 is the oxygen of the crystalline water and combines two H3 atoms. Accordingly, the reasonable formula is $Nd_2B_6O_{10}(OH)_4•H_2O$.

As shown in Figure 1, B1 is 3-fold coordinated by O1, O5, and O6; B2 and B3 are tetrahedrally coordinated by O2, O3, O5, O7, and O1, O3, O7, O4, respectively. All the bond distances and angles are in the normal range (Table 2). The FBB in borate net is a three-membered ring (3MR) $[B_3O_6(OH)_2]^{5-}$, which can be expressed as 3: [(3: Δ + 2T)].[33,34] Such a 3MR FBB is found in a number of polyborates.[35,36] In $Nd_2B_6O_{10}(OH)_4•H_2O$, each FBB is connected to two neighbors via common oxygen atoms O3, forming an infinite $[B_3O_5(OH)_2]^{3-}$ chain along the *b*-axis. The further linkage of the borate chains is by hydrogen bonds via hydroxyl groups of the chains and the crystallized water molecules. The connection by hydrogen bonds O6−H2···O1, O4−H1···O8, and O8−H3···O6 gives rise to the 2-D layer $[B_6O_{10}(OH)_4•H_2O]^{6-}$. The distances of O6−O1, O4−O8, and O8−O6 are 2.706, 2.707, and 2.743 Å, respectively, which are typical for hydrogen bonds.[37]

In the structure of $Nd_2B_6O_{10}(OH)_4•H_2O$, Nd^{3+} atom is coordinated by 8 oxygen atoms (one of them is a hydroxyl group) in an irregular environment with Nd−O distances in the range of 2.386 to 2.764 Å. Each $NdO_7(OH)$ polyhedron

(33) Christ, C. L.; Clark, J. R. *Phys. Chem. Miner.* **1977**, *2*, 59–87.
(34) Burns, P. C.; Grice, J. D.; Hawthorne, F. C. *Can. Mineral.* **1995**, *22*, 1131–1151.
(35) Burns, P. C.; Hawthorne, F. C. *Can. Mineral.* **1993**, *31*, 297–304.
(36) Yamnova, N. A.; Egorov-Tismenko, Y. K.; Malinko, S. V.; Pushcharovskii, D. Y.; Dorokhova, G. I. *Kristallografiya* **1994**, *39*, 991–993.
(37) Emsley, J. *Chem. Soc. Rev.* **1980**, *9*, 91–124.

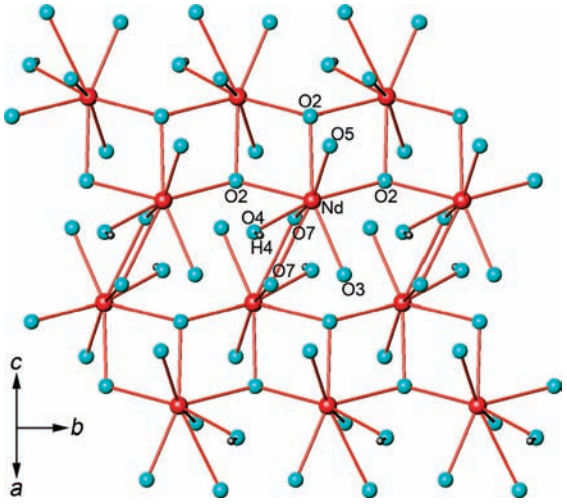

Figure 2. Connection of NdO_8 polyhedra along the [101] direction.

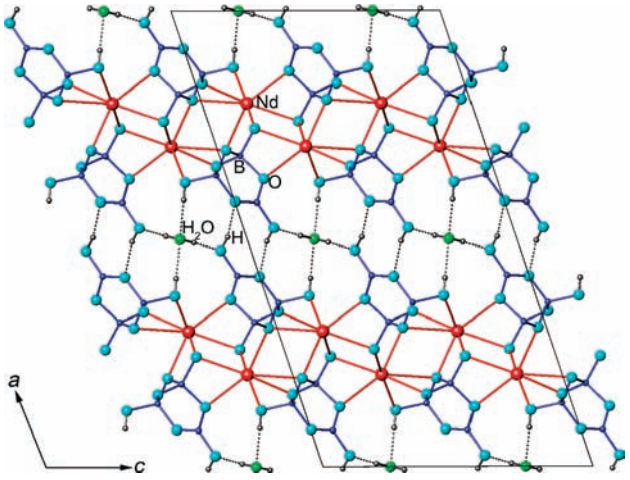

Figure 3. Projection of the structure of $Nd_2B_6O_{10}(OH)_4 \bullet H_2O$ along the [010] direction.

connects to three $NdO_7(OH)$ polyhedra by edge-sharing and two $NdO_7(OH)$ polyhedra via corner-sharing, forming a corrugated two-dimensional $[NdO_4(OH)]^{6-}$ layer, as shown in Figure 2. The $[NdO_4(OH)]^{6-}$ layer connects to the neighboring borate chains by sharing O2, O3, O4. and O7 atoms, forming the 3-D structure, as shown in Figure 3.

In the IR spectrum of $Nd_2B_6O_{10}(OH)_4 \bullet H_2O$ (Figure 4), the broad absorption band at about 3650−2750 cm^{-1} is related to the stretching vibrations of O−H groups, showing that the strengths of the hydrogen bonds are comparable to those in the ice.[37,38] The peak at 1670 cm^{-1} is assigned to the bending vibration mode of O−H groups from crystalline water H3−O8−H3,[39] which is "locked" by four hydrogen bonds toward to the adjacent layers, so the oxygen atom O8 has a relatively small thermal displacement factor (Table 2). It is the interaction of the hydrogen bonds (represented in dotted gray lines) that hold the borate chains together. The incorporation of the water molecules in constructing the structure reflects that a certain amount of water is necessary for the formation of

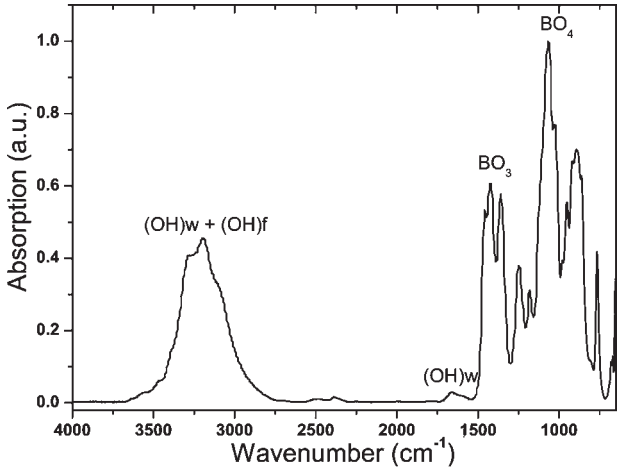

Figure 4. IR spectrum of $Nd_2B_6O_{10}(OH)_4 \bullet H_2O$. (OH)w and (OH)f represent the hydroxyl groups from crystalline water and framework respectively.

the title compounds. The vibration bands at about 1400−1100 cm^{-1} and 1100−800 cm^{-1} are generally assigned to the vibration of BO_3 and BO_4 groups, respectively.[40]

$Ln_2B_6O_{10}(OH)_4 \bullet H_2O$ (*Ln* = Pr, Sm, Eu, Gd, Dy, Ho, and Y) are isostructural to $Nd_2B_6O_{10}(OH)_4 \bullet H_2O$. The unit cell parameters of these compounds are obtained by profile fitting using program TOPAS,[41] and the refined results are listed in Table 4. It is shown that the parameters decrease gradually from Pr to Dy to Y and Ho with a decrease in the rare earth ionic radius.

3.3. Thermal Behavior and IR Investigation. The thermal behaviors of the $Ln_2B_6O_{10}(OH)_4 \bullet H_2O$ compounds are similar, and all of the compounds dehydrate in three steps between 50 and 800 °C, as detected by the TG analysis (Figure 5 and Figure S2 of the Supporting Information). Here, $Sm_2B_6O_{10}(OH)_4 \bullet H_2O$ is discussed as a representative (Figure 5b). The three steps correspond to the removal of the crystalline water molecules between 50 and 400 °C, dehydration of half hydroxyl groups between 400 and 550 °C, and the further dehydration of the remaining hydroxyl groups between 550 and 720 °C respectively. The signals corresponding to H_2O and OH species are also detected in situ by mass spectra (Figure 5b). The total weight loss of $Sm_2B_6O_{10}(OH)_4 \bullet H_2O$ to anhydrous product SmB_3O_5 is 9.07 wt % (calcd 8.83 wt %).

The products obtained by thermal treatment of the as-synthesized $Sm_2B_6O_{10}(OH)_4 \bullet H_2O$ samples under different temperatures are shown in Figure 6. The loss of the crystalline water at 300 °C produces a new compound $Sm_2B_6O_{10}(OH)_4$, which exhibits a similar diffraction pattern with the parent compound. The peak profile fitting of the XRD data of $Sm_2B_6O_{10}(OH)_4$ indicates a monoclinic lattice with the constants a = 21.7896(9), b = 4.3616(1), c = 11.9504(3) Å, β = 109.585(2)°, and V = 1070.03(6) $Å^3$. These parameters are close to those of the as-synthesized $Sm_2B_6O_{10}(OH)_4 \bullet H_2O$ (a = 21.698, b = 4.363, c = 12.076 Å, β = 108.44°, and V = 1084.65 $Å^3$, see Table 4). It is expected that the framework of the structure is maintained after the

(38) Hammer, V. M. F.; Libowitzky, E.; Rossman, G. R. *Am. Mineral.* **1998**, *83*, 569–576.
(39) Dean, J. A. *Lange's Handbook of Chemistry*, 15th ed.; McGraw-Hill Book Co.: New York, 1999; pp 7−45.
(40) Laperches, J. P.; Tarte, P. *Spectrochim. Acta* **1966**, *22*, 1201.
(41) *TOPAS V2.1, General Profile and Structure Analysis Software for Powder Diffraction Data*; Bruker AXS: Karlsruhe, Germany,2003.
(42) Dong, C. J. *Appl. Crystallogr.* **1999**, *32*, 838.

Table 4. Unit Cell Parameters of $Ln_2B_6O_{10}(OH)_4{\bullet}H_2O$

compound	a (Å)	b (Å)	c (Å)	β (deg)	V (Å^3)
$Pr_2B_6O_{10}(OH)_4{\bullet}H_2O$	21.804(3)	4.3780(3)	12.2875(9)	108.236(6)	1114.0(2)
$Nd_2B_6O_{10}(OH)_4{\bullet}H_2O$	21.756(4)	4.3671(9)	12.192(2)	108.29(3)	1099.9(4)
$Sm_2B_6O_{10}(OH)_4{\bullet}H_2O$	21.6980(6)	4.3633(1)	12.0765(2)	108.437(1)	1084.65(4)
$Eu_2B_6O_{10}(OH)_4{\bullet}H_2O$	21.678(2)	4.3569(2)	12.0113(5)	108.423(3)	1076.3(1)
$Gd_2B_6O_{10}(OH)_4{\bullet}H_2O$	21.667(2)	4.3524(2)	11.9364(6)	108.337(3)	1070.5(1)
$Dy_2B_6O_{10}(OH)_4{\bullet}H_2O$	21.651(2)	4.3388(2)	11.8237(6)	108.354(4)	1054.2(1)
$Y_2B_6O_{10}(OH)_4{\bullet}H_2O$	21.625(2)	4.3318(3)	11.7620(8)	108.360(6)	1045.7(2)
$Ho_2B_6O_{10}(OH)_4{\bullet}H_2O$	21.63(2)	4.328(2)	11.701(5)	108.44(3)	1039(1)

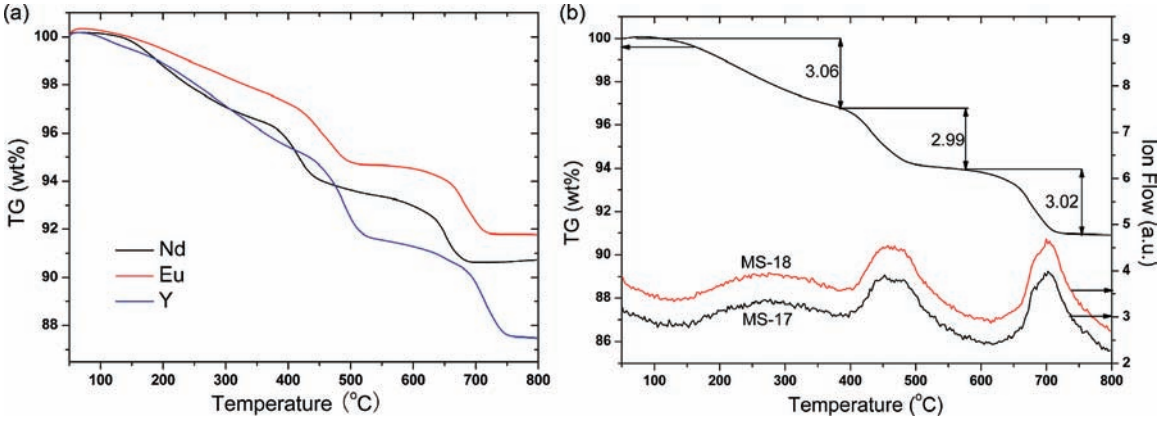

Figure 5. (a) TG curves of as-synthesized $Ln_2B_6O_{10}(OH)_4{\bullet}H_2O$ (Ln = Nd, Eu, and Y); (b) TG-MS curves of as-synthesized $Sm_2B_6O_{10}(OH)_4{\bullet}H_2O$.

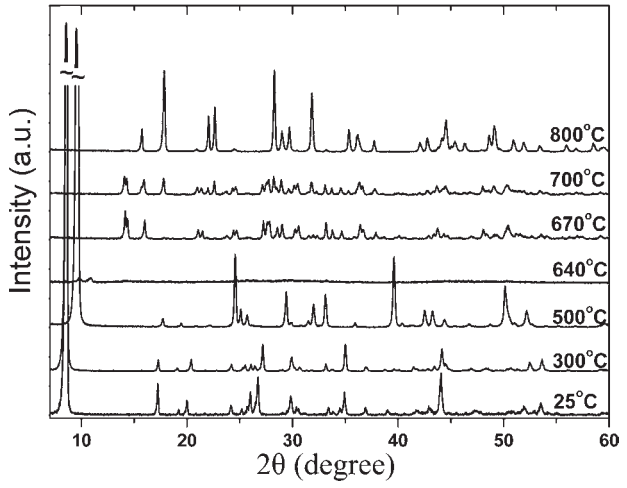

Figure 6. X-ray diffraction patterns of as-synthesized $Sm_2B_6O_{10}(OH)_4{\bullet}H_2O$ (25 °C) and its calcined products at different temperatures.

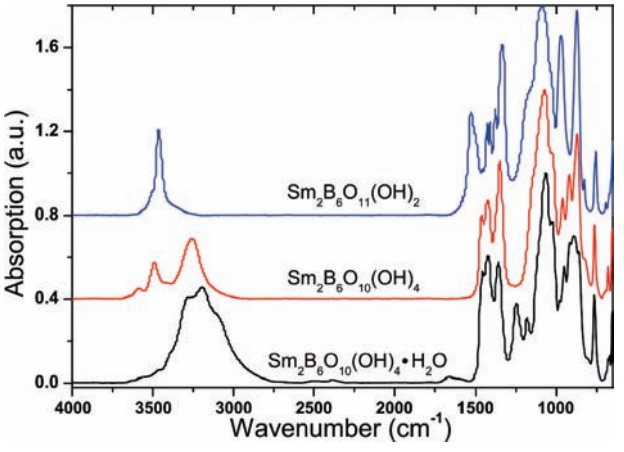

Figure 7. IR spectra of as-synthesized $Sm_2B_6O_{10}(OH)_4{\bullet}H_2O$ and its dehydrated products $Sm_2B_6O_{10}(OH)_4$ and $Sm_2B_6O_{11}(OH)_2$.

removal of the crystalline water and the change of cell parameter originating from the slight adjustment of the borate layer, though the details of the structure of $Sm_2B_6O_{10}(OH)_4$ are remained unknown. The $Sm_2B_6O_{10}(OH)_4$ sample was kept under water-saturated atmosphere at room temperature for 10 h to test its absorbability for water molecules. The experimental result showed that $Sm_2B_6O_{10}(OH)_4$ did not readsorb water.

It is noteworthy that the hydrogen bond plays an important role in the formation of the borate layer in the structure of $Sm_2B_6O_{10}(OH)_4{\bullet}H_2O$. The removal of water molecules destroys the original hydrogen bonds O4−H4···O8 and O8−H8···O6, which leads to a reorganization of the hydroxyl groups, resulting in new hydrogen bonds between O4 and O6 (or O5) atoms. The IR spectra spectrum of $Sm_2B_6O_{10}(OH)_4$ is shown in Figure 7, where the characteristic absorption peak at 1670 cm^{-1} relating to the bending vibration of O−H groups of the crystalline water disappears. In the spectrum, there are three peaks at 3590, 3490, and 3260 cm^{-1} relating to O−H stretching vibrations. The first peak is weak and may relate to a small part of disengaged O−H groups. The absorption bands at 3490 and 3260 cm^{-1} may relate to the new hydrogen bonds and the remaining hydrogen bonds of O6−H6···O1, respectively.

At about 500 °C, half of the hydroxyl groups in the structure of $Sm_2B_6O_{10}(OH)_4$ are removed, which results in the formation of $Sm_2B_6O_{11}(OH)_2$. $Sm_2B_6O_{11}(OH)_2$ shows a new set of diffraction patterns (Figure 6), and the profile can be indexed in a C-centered monoclinic lattice with a = 18.171(5), b = 4.358(8), c = 11.925(1) Å, β = 89.88(6)°, and V = 944.3(2) Å^3. Axis a shrinks considerably, the β angle decreases, and the axes of b and c have almost no

change. The change of the unit cell is understandable because the hydrogen bonds in the structure are orientated along the *a*-direction. The condensation process may also be accompanied by a shift of the *bc* layer. In the IR spectrum of $Sm_2B_6O_{11}(OH)_2$ (Figure 7), there remains only one sharp peak around 3470 cm^{-1}, corresponding to O−H stretching vibration.

Increasing temperature to 640 °C leads to further dehydration, resulting in an amorphous phase (Figure 7). At 670 °C, the amorphous phase undergoes crystallization to a mixture of triclinic $SmBO_3$ and α-SmB_5O_9. These two phases react at higher temperature (800 °C), forming α-SmB_3O_6.

The other compounds, $Ln_2B_6O_{10}(OH)_4•H_2O$ (*Ln* = Pr, Eu, Gd, Dy, Ho and Y), exhibit similar dehydration behavior in the first two steps, giving rise to $Ln_2B_6O_{10}(OH)_4$ and $Ln_2B_6O_{11}(OH)_2$, respectively. The final anhydrous products after the third dehydration step are different. The distribution of the products during the dehydration processes of $Ln_2B_6O_{10}(OH)_4•H_2O$ is summarized in Figure 8. Clearly, they can be divided into four categories with a decrease in radii of the rare earth cations: for *Ln* = Pr, $Pr_2B_6O_{11}(OH)_2$ converts to α-PrB_3O_6; for *Ln* = Nd, a mixture of triclinic $NdBO_3$, α-NdB_3O_6, and amorphous phase forms first, and the triclinic $NdBO_3$ reacts with the amorphous phase to form α-NdB_3O_6 at higher temperature; for *Ln* = Sm, Eu, Gd, $Ln_2B_6O_{11}(OH)_2$ produce α-LnB_3O_6, with an intermediated stage containing $LnBO_3$, α-LnB_5O_9, and α-LnB_3O_6; for *Ln* = Dy, Ho, and Y, hexagonal $LnBO_3$ form above 650 °C, and the products are consistent with the previous studies on the binary $Ln_2O_3-B_2O_3$ (*Ln* = Pr, Dy, Ho, and Y) systems.[5,6]

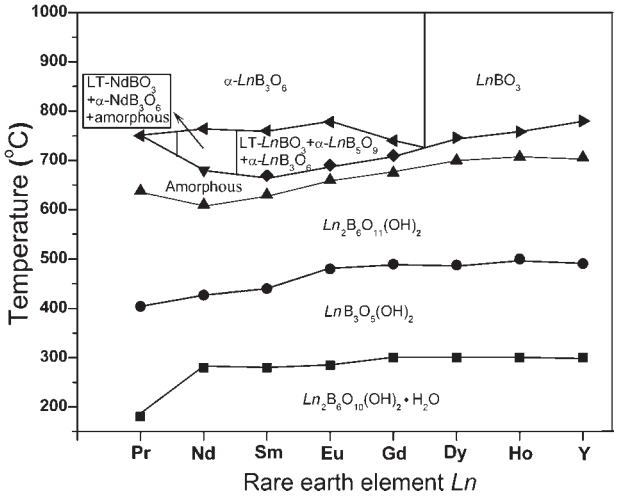

Figure 8. Phase relations during the dehydration process of $Ln_2B_6O_{10}(OH)_4•H_2O$.

3.4. Luminescent Property. A series of europium-doped samples $Gd_{2-2x}Eu_{2x}B_6O_{10}(OH)_4•H_2O$ (x = 0.01−1.00) were prepared for the study of luminescent property. The excitation spectra (Figure 9a) were measured from 200 to 550 nm by monitoring the Eu^{3+} emission at 613 nm. In the excitation spectra of $Gd_{2-2x}Eu_{2x}B_6O_{10}(OH)_4•H_2O$

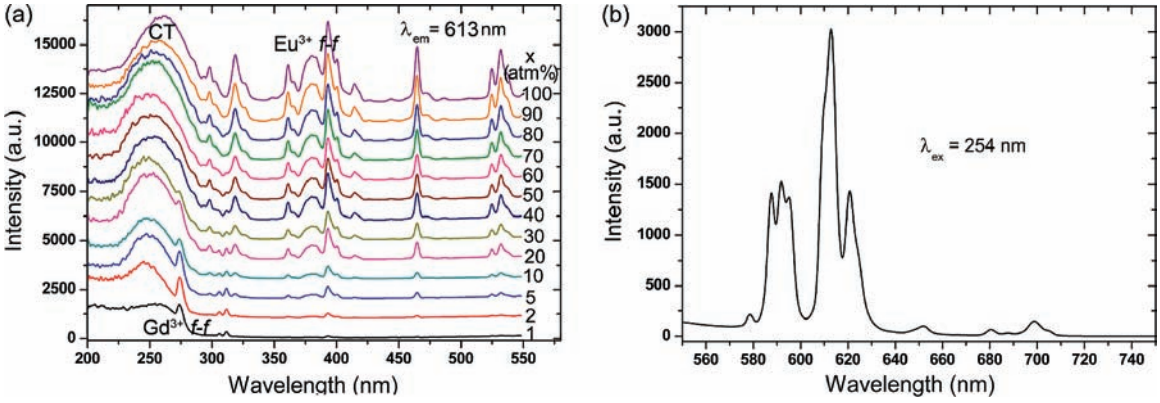

Figure 9. (a) Excitation spectra of $Gd_{2-2x}Eu_{2x}B_6O_{10}(OH)_4•H_2O$ (x = 0.01−1.00) samples; (b) emission spectrum of the $Gd_{2-2x}Eu_{2x}B_6O_{10}(OH)_4•H_2O$ (x = 0.01) sample.

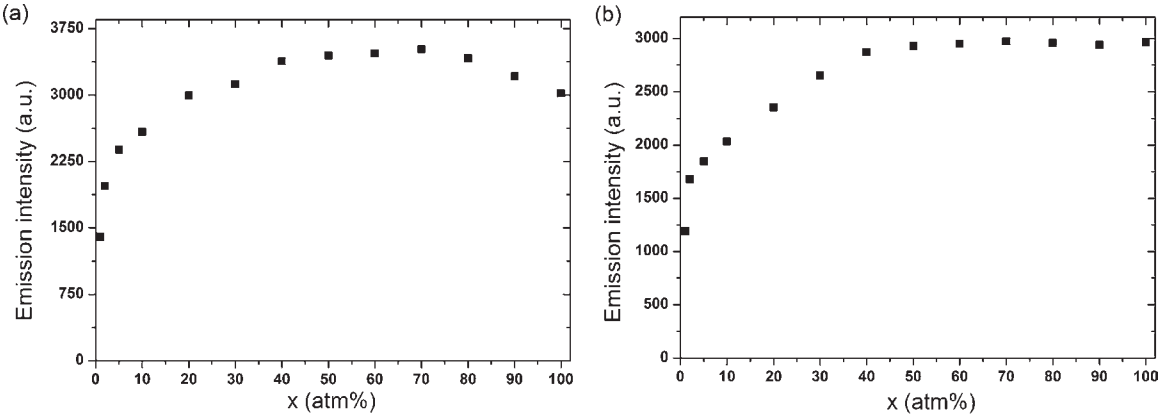

Figure 10. Dependence of the emission intensity at 613 nm with the doping amount x in $Gd_{2-2x}Eu_{2x}B_6O_{10}(OH)_4•H_2O$ (x = 0.01−1.00).

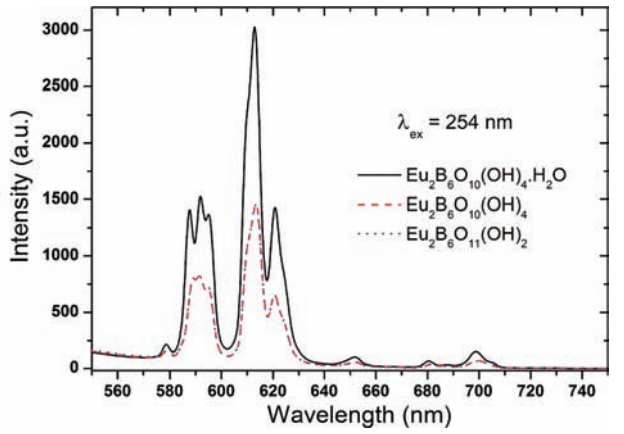

Figure 11. Emission spectra of as-synthesized $Eu_2B_6O_{10}(OH)_4 \bullet H_2O$ and its dehydrated products $Eu_2B_6O_{10}(OH)_4$ and $Eu_2B_6O_{11}(OH)_2$.

($x = 0.01-0.60$), the broad band at about 220−290 nm is the typical absorption of charge transfer (CT) of $O \rightarrow Eu^{3+}$; the narrow peaks in the wavelenth range of 298−550 nm originate from Eu^{3+} $f-f$ transitions; and the narrow peaks at 274, 306, and 312 nm are from the $^8S_{7/2}-^6I_J$, $^8S_{7/2}-^6I_{5/2}$, and $^8S_{7/2}-^6P_{7/2}$ transitions of Gd^{3+}, respectively.[43,44] The appearance of Gd^{3+} absorption in the excitation spectra indicates that there is an energy transfer from Gd^{3+} to Eu^{3+} in this series of compounds.[44] With an increase in Eu^{3+} concentration ($x = 0.70-0.90$), the absorption of the CT band becomes stronger, which overlaps with the $^8S_{7/2}-^6I_J$ transitions of Gd^{3+}. Meanwhile, the intensities of the $f-f$ excitation peaks of Eu^{3+} increase accordingly and become comparable with that of the CT band in pure $Eu_2B_6O_{10}(OH)_4 \bullet H_2O$. The strong $f-f$ excitation is largely due to the irregular coordination of Eu^{3+} ion in the structure.

The emission spectrum of the $Gd_{2-2x}Eu_{2x}B_6O_{10}(OH)_4 \bullet H_2O$ ($x = 0.01$) sample is shown in Figure 9b. Five groups of emission peaks at 578, 580−600, 600−640, 640−660, and 670−710 nm were observed, which can be attributed to the $^5D_0 \rightarrow {}^7F_J$ transitions with $J = 0-4$ of Eu^{3+} ion, respectively.[45] The $^5D_0 \rightarrow {}^7F_0$ (578 nm) is a single peak, which is consistent with the single crystallographic site of Eu^{3+} ion in the structure. The intensity of the peak at 592 nm ($^5D_0 \rightarrow {}^7F_1$, a magnetic dipole−dipole transition) is weaker than that of 620 nm ($^5D_0 \rightarrow {}^7F_2$, an electric dipole−dipole transition), which agrees with the ancentrosymmetric coordination environment of Eu^{3+} in the structure.

The influence of Eu^{3+} concentration on the intensity of the emission peak 613 nm is shown in Figure 10. When excited by 254 nm (CT of $O^{2-} \rightarrow Eu^{3+}$), the emission intensity increases with the Eu^{3+} concentration first. It reaches a maximum value in the range of $x = 0.50-0.80$ and then decreases slightly in the high Eu^{3+} concentration (Figure 10a). If excited by 393 nm ($f-f$ transition of Eu^{3+}), the emission intensity reaches a maximum value and then maintains almost constant in the range of $x = 0.60-1.00$ (Figure 10b). The saturation of the intensities with an increase in the Eu^{3+} concentration is due to interaction of the activeted centers by the cross-relaxation or energy tranfer between exited and unexcited Eu^{3+} ions. In this series of compounds $Gd_{2-2x}Eu_{2x}B_6O_{10}(OH)_4 \bullet H_2O$ ($x = 0.01-1.00$), the quenching effect seems quite weak, corresponding to the saturation appearing at higher Eu^{3+} content. If the quenching effect is stronger than the increase in the exited centers, the emission intensity decreases with a further increase in Eu^{3+} concentration, as that under $O^{2-} \rightarrow Eu^{3+}$ charge transfer excitation; on the other hand, if the quenching effect is comparble with an increase in the exited centers, the intensity exhibits a simple saturation, as observed that under the $f-f$ excitation.

In Figure 11, we compare the luminescent spectra of the dehydrated compounds $Eu_2B_6O_{10}(OH)_4$ and $Eu_2B_6O_{11}(OH)_2$ with the parent compound $Eu_2B_6O_{10}(OH)_4 \bullet H_2O$. The similar excitation and emission spectra indicate the similar coordination environments of Eu^{3+} in these compounds, which also implies that the $[LnO_5]^{7-}$ layer in the structures remains during the two dehydration processes. Generally, an increase in luminescence intensity is expected in the stepwise dehydration due to diminution of nonradiative deactivation via the O−H vibration. However, we observed that the luminescence intensities of the dehydrated products are weaker than their parent compounds. Because the luminescent property strongly depends on the structure of the compounds, the poor crystallinities of the dehydrated products may be responsible for the decrease in the luminescent intensities. The high efficiency of the $f-f$ transitions indicates that $Eu_2B_6O_{10}(OH)_4 \bullet H_2O$ and its dehydrated products, $Eu_2B_6O_{10}(OH)_4$ and $Eu_2B_6O_{11}(OH)_2$, might be potential red luminescent materials.

4. Conclusion

A new series of hydrous rare earth borates $Ln_2B_6O_{10}(OH)_4 \bullet H_2O$ (*Ln* = Pr, Nd, Sm, Eu, Gd, Dy, Ho, and Y) were synthesized under hydrothermal conditions. The structure of $Nd_2B_6O_{10}(OH)_4 \bullet H_2O$ was determined by single-crystal XRD technique. It crystallizes in the monoclinic space group $C2/c$ with lattice constants $a = 21.756(4)$, $b = 4.3671(9)$, $c = 12.192(2)$ Å, and $\beta = 108.29(3)°$. The other rare earth borates are isostructural to $Nd_2B_6O_{10}(OH)_4 \bullet H_2O$ as confirmed by powder X-ray profile fitting. The fundamental building block (FBB) in the structure is the three-membered ring $[B_3O_6(OH)_2]^{5-}$. The FBBs are connected by sharing oxygen atoms forming an infinite $[B_3O_5(OH)_2]^{3-}$ chain, which is further linked by hydrogen bonds forming a two-dimensional $[B_6O_{10}(OH)_4 \bullet H_2O]^{6-}$ layer. $Ln_2B_6O_{10}(OH)_4 \bullet H_2O$ loses water molecules stepwise, forming two new phases $Ln_2B_6O_{10}(OH)_4$ and $Ln_2B_6O_{11}(OH)_2$. The final products after the third dehydration process are known anhydrous rare earth borates. $Gd_{2-x}Eu_{2x}B_6O_{10}(OH)_4 \bullet H_2O$ ($x = 0.01-1.00$) exhibits high efficient Eu^{3+} $f-f$ transitions and energy transfer from Gd^{3+} to Eu^{3+}. $Eu_2B_6O_{10}(OH)_4 \bullet H_2O$ and its two dehydrated products $Eu_2B_6O_{10}(OH)_4$ and $Eu_2B_6O_{11}(OH)_2$ have similar excitation and emission spectra. These compunds may be potential red phosphors.

Acknowledgment. This work is financially supported by the State Science and Technology Commission of China

(43) Wang, J. G.; Jing, X. P.; Yan, C. H.; Lin, J. H. *J. Electrochem. Soc.* **2005**, *152*, G186–G188.
(44) You, F. T.; Yang, Z.; Lu, P. C.; Wang, Y. X.; Lin, J. H.; Tao, Y. *High Energy Phys. Nucl. Phys.* **2001**, *25*, 70–74.
(45) Yang, Z.; Lin, J. H.; Su, M. Z.; You, L. P. *Mater. Res. Bull.* **2000**, *35*, 2173–2182.

(2010CB833103) and the National Natural Science Foundation of China (NSFC 20821091).

Supporting Information Available: Powder X-ray diffraction profile of the unknown phase, which often exists as an impurity for the synthesis of $Ln_2B_6O_{10}(OH)_4 \bullet H_2O$ (*Ln* = Y, Dy, and Ho), is shown in Figure S1; TG curves of the as-synthesized $Ln_2B_6O_{10}(OH)_4 \bullet H_2O$ (*Ln* = Pr, Sm, Gd, Dy, and Ho) are shown in Figure S2. This material is available free of charge via the Internet at http://pubs.acs.org.